

Phase-stable source of high-quality three-photon polarization entanglement by cascaded down-conversion

Zachary M. E. Chaisson ¹, Patrick F. Poitras ¹, Micaël Richard ¹, Yannick Castonguay-Page,^{2,1} Paul-Henry Glinel ¹,
Véronique Landry ¹ and Deny R. Hamel ¹

¹*Département de physique et d'astronomie, Université de Moncton, Moncton, New Brunswick, E1A 3E9 Canada*

²*Department of Physics and Astronomy, McMaster University, Hamilton, Ontario, L8S 4L8 Canada*



(Received 12 August 2021; revised 20 February 2022; accepted 24 March 2022; published 3 June 2022)

Stable sources of entangled photons are important requirements for quantum communications. In recent years, cascaded down-conversion has been demonstrated as an effective method of directly producing three-photon entanglement. However, to produce polarization entanglement these sources have until now relied on intricate active phase stabilization schemes, thus limiting their robustness and usability. In this paper, we present a completely phase-stable source of three-photon entanglement in the polarization degree of freedom. With this source, which is based on a cascade of two pair sources based on Sagnac configurations, we produce states with over 96% fidelity with an ideal Greenberger-Horne-Zeilinger state. Moreover, we demonstrate the stability of the source over several days without any ongoing optimization. We expect this source to be a useful tool for applications requiring multiphoton entanglement, such as quantum secret sharing and producing heralded entangled photon pairs.

DOI: [10.1103/PhysRevA.105.063705](https://doi.org/10.1103/PhysRevA.105.063705)

I. INTRODUCTION

Multiphoton entanglement is an important resource for a wide range of quantum information applications [1]. Three-photon Greenberger-Horn-Zeilinger (GHZ) states in particular are known to be useful for tasks such as quantum secret sharing [2], quantum anonymous transfer [3], and optical quantum computing [4]. Currently, multiphoton entangled states are most often produced by combining two or more entangled photon pairs from spontaneous parametric down-conversion (SPDC) and using postselection to project onto the desired states [5–16]. In this approach, postselection is fundamental to the state creation process, as photons must first be detected in order to produce the desired entangled state.

An alternative approach to produce three-photon states, without relying on these postselection methods, is to instead cascade two SPDC sources (C-SPDC) to directly create the desired state [17]. This novel approach has already been successfully employed to produce photon triplets using separate sources [18,19] as well as with a cascade within a single integrated device [20].

C-SPDC has also been used to produce polarization entanglement and to herald Bell states [21]. However, demonstrations of polarization entanglement using C-SPDC have, until now, used Mach-Zehnder interferometer configurations. This type of configuration has the advantage of only using the crystals in a single direction, which allows for the use of waveguided crystals pigtailed with single-mode fibers optimized for the pump at the entrance and the down-converted signal at the output. However, it also has the significant drawback of requiring active stabilization of the phase between the crystals in each arm, which adds significant complexity

to the setup and reduces its robustness in real-world applications. An alternative to the Mach-Zehnder configuration is to instead employ a Sagnac interferometer, removing the need for active stabilization but losing the advantage of optimized single-mode fibers.

In this paper, we present a phase-stable source of polarization-entangled photon triplets based on C-SPDC. By cascading two sources built using a Sagnac interferometer [22,23], which are inherently phase stable, we construct a source which can display high state fidelity with GHZ states without active stabilization.

II. EXPERIMENTAL SETUP

The state we aim to produce through C-SPDC is the three-photon GHZ state, given by

$$|\text{GHZ}\rangle = \frac{1}{\sqrt{2}}(|HHH\rangle + |VVV\rangle), \quad (1)$$

where $|HHH\rangle$ represents three photons with horizontal polarization, while $|VVV\rangle$ represents vertical polarization.

We start by creating two independent SPDC sources, as seen in Fig. 1(a). In the first source, a periodically poled potassium triphosphate (PPKTP) crystal is placed in a Sagnac interferometer. This source uses a type-II SPDC process to create states of the form

$$|\Psi^\pm\rangle = \cos\theta |HV\rangle + e^{i\phi} \sin\theta |VH\rangle, \quad (2)$$

where θ and ϕ are determined by the polarization of the pump. These two parameters are controlled by turning a half-wave plate (HWP) and tilting a quarter-wave plate (QWP), respectively.

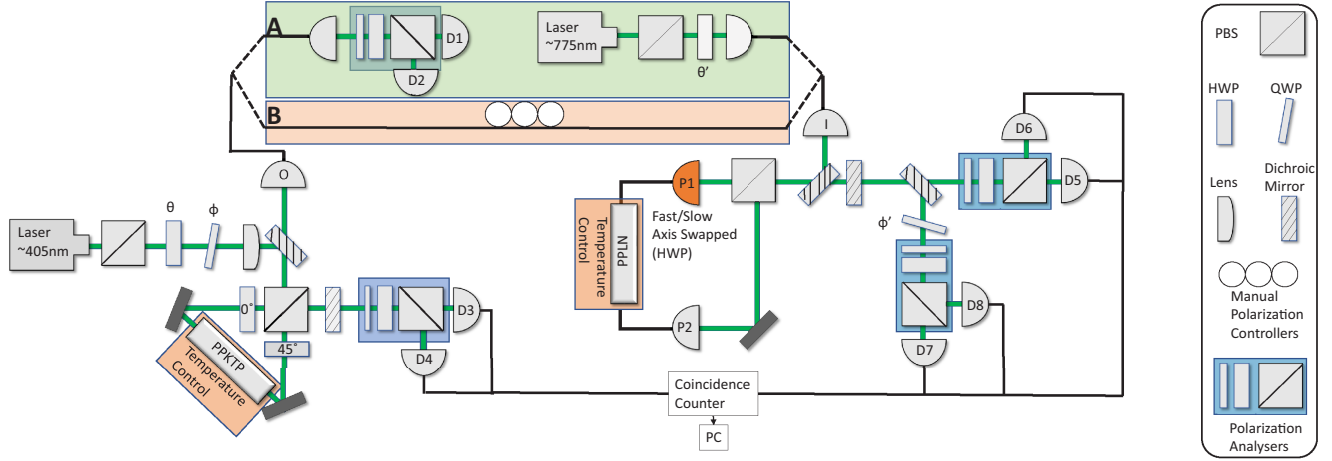


FIG. 1. Experimental setup used to create and measure entangled photon pairs (A) or triplets (B). In the first source, a 405-nm grating-stabilized laser diode (Toptica Topmode) pumps a PPKTP crystal (Raicol), which is heated at 48.0 °C to produce photons at 777 and 846 nm. The PPKTP crystal is placed inside a Sagnac interferometer, along with superachromatic half-wave plates (Thorlabs SAHWP05M-700). After filtering out the pump with dichroic mirrors, the resulting state is that of Eq. (2). The 846-nm photon is sent to polarization analyzers, whereas the 777-nm photon is coupled into a single-mode fiber by collimator O and is either measured directly (A) or sent to the second source after passing through a manual polarization controller (B). In the second source, a PPLN waveguide is pumped either directly by a wavelength-tunable grating-stabilized laser diode (Sacher Lynx TEC 150, Littrow Series) to produce the state in Eq. (3) (A), or by 777-nm single photons from the first source to produce Eq. (4) (B). The PPLN waveguide is heated at 50.0 °C to produce photon pairs at approximately 1530 and 1570 nm. The fast and slow axes of the collimator P1 (in orange) are swapped to mimic the effects of a half-wave plate at 45°. All photons are detected using superconducting nanowire single-photon detectors (SNSPDs, Photon Spot).

For the second source, a type-0 periodically poled lithium niobate (PPLN) crystal waveguide, pigtailed at each end with polarization maintaining fibers, is placed in a Sagnac interferometer. Since the crystal is pumped from both directions, it is not possible to use fibers optimized for the pump wavelength.

Instead, we employ polarization-maintaining fibers which are single mode for the down-converted photons [24], with angled physical contact ferrule connectors to avoid back reflections. The state we aim to produce has the form

$$|\Phi^\pm\rangle = \cos\theta' |HH\rangle + e^{i\phi'} \sin\theta' |VV\rangle, \quad (3)$$

where again the weighing of the terms θ' and phase ϕ' can be set respectively by turning a HWP and tilting a QWP, although in this source the phase is set by acting on the down-converted photons rather than on the pump.

The two sources are combined by using one of the photons from the PPKTP source as a pump for the PPLN source, as seen in Fig. 1(b). A photon in the state $|H\rangle$ is down-converted into the state $|VV\rangle$ while the mode $|V\rangle$ is down-converted to $|HH\rangle$. The resulting state that we obtain is of the form

$$|\text{GHZ}\rangle_{\text{expt}} = \cos\theta |HHH\rangle + e^{i\Phi(\phi,\phi')} \sin\theta |VVV\rangle. \quad (4)$$

III. STATE PREPARATION

To prepare the desired state, we start with separated sources as shown in Fig. 1(a). This allows us to first optimize each pair source separately.

The two sources are then connected, as shown in Fig. 1(b), to form the cascaded source. The manual polarization controller is adjusted so that the horizontal and vertical polarizations are conserved between collimators O and I.

The angle of the HWP θ is set to produce $|HHH\rangle$ and $|VVV\rangle$ with equal probability. This angle is calculated to compensate for any imbalance in coupling efficiency between photons traveling clockwise and counterclockwise in the Sagnac loops, as measured from photon pairs.

With the balance set, we can focus on controlling the phase of the state. We start by performing a $\sigma_x \otimes \sigma_x \otimes \sigma_x$ measurement on the photon triplets, where σ_x is the Pauli X matrix, while varying the phase ϕ . These results are given in Fig. 2. As expected, we find a sinusoidal dependence for $\langle \sigma_x \otimes \sigma_x \otimes \sigma_x \rangle$, with the fit having a visibility of 0.92 ± 0.06 .

IV. RESULTS

We first characterize the pair sources independently. Using maximum-likelihood quantum state tomography [25], we reconstruct the density matrices of the two entangled photon pairs from both sources. Photons in each output mode are projected onto one of three mutually unbiased polarization bases, (horizontal and vertical, circular right and circular left, diagonal right and diagonal left) for a total of six different polarization measurements per output mode. For pairs, this leads to 36 measurement combinations. The measured coincidence counts are shown in Tables I and II while the results of the tomography are shown in Fig. 3.

Detector dark counts, determined by turning off the pump lasers, average approximately five counts per second on each detector channel. These are not subtracted for any measurement presented in this paper. The twofold coincidences measured at the detectors from the PPKTP source number $R_{\text{pairs}} = 3 \times 10^5$ per second with a pump power of 9.4 mW at the entrance of the interferometer. From the tomography, we find the source produces a $|\Psi^-\rangle$ state with a fidelity

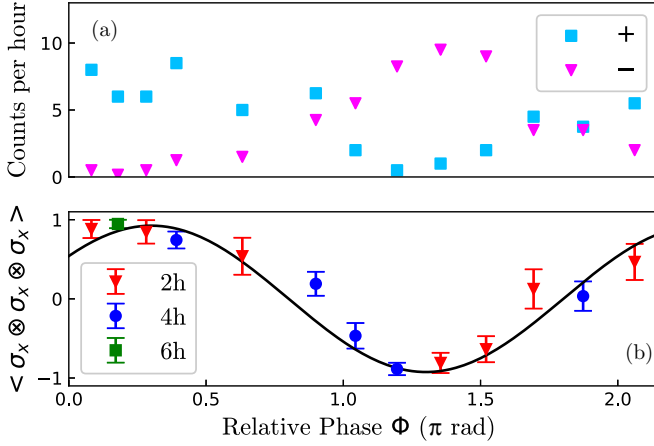


FIG. 2. Determination of the phase necessary to create the desired GHZ state. By tilting the QWP we can change the relative phase of our state. This is reflected in (b) the measured value of the expectation value of the Pauli X triplet measurement. The black line is a weighted sinusoidal fit, where the phase and amplitude are left as fitting parameters. The fit has an amplitude of 0.92 ± 0.06 . The total length of each measurement is displayed in the legend. The error bars are one standard deviation and calculated by assuming Poissonian count rates. The obtained triplet coincidence rates are normalized per hour and displayed in (b). The values contributing positively to the σ_x measurement are in cyan, while the negative contributions are in magenta. From these rates, we determine that the triplet coincidences are detected at a rate of 8.3 ± 0.5 per hour.

of $96.45 \pm 0.01\%$. The PPLN source produces 1.5×10^4 twofold coincidences per second with a pump power of approximately $1 \mu\text{W}$ at the entrance of the crystal. From the tomography we find that the source produces a $|\Phi^+\rangle$ state with a fidelity of $95.06 \pm 0.05\%$. From the ratio of single-photon detections to twofold coincidence detections, the averages of the combined coupling and detection efficiencies are determined to be $\eta_{846} = 0.30 \pm 0.02$, $\eta_{1530} = 0.16 \pm 0.01$, and $\eta_{1570} = 0.13 \pm 0.01$ for the 84-, 1530-, and 1570-nm photons, respectively. Coupling efficiencies from collimator I to collimators P1 and P2 are measured at $\eta_I = 0.30 \pm 0.02$ from single-photon detection rates. The rate of photons produced by the cascaded sources is given by [18]

$$R_{\text{triplets}} = \frac{P_{\text{PPLN}} R_{\text{pairs}} \eta_I \eta_{1530} \eta_{1570}}{\eta_{D777}}, \quad (5)$$

where $\eta_{D777} = 0.79 \pm 0.03$ is the estimated detection efficiency of the SNSPD measuring the 777-nm photons during

TABLE I. Measured coincidence counts for the tomography of the PPKTP source.

	<i>H</i>	<i>V</i>	<i>D</i>	<i>A</i>	<i>R</i>	<i>L</i>
<i>H</i>	6725	574095	314314	268339	250258	330138
<i>V</i>	629929	8511	277541	347720	349167	282803
<i>D</i>	294404	311773	12154	598738	237235	332825
<i>A</i>	361676	273644	603285	18103	378080	289123
<i>R</i>	370125	238506	358322	238276	31821	601607
<i>L</i>	275723	339252	288303	327764	577284	10753

TABLE II. Measured coincidence counts for the tomography of the PPLN source.

	<i>H</i>	<i>V</i>	<i>D</i>	<i>A</i>	<i>R</i>	<i>L</i>
<i>H</i>	39844	722	18622	21781	15142	22592
<i>V</i>	698	41173	29202	22077	26405	19971
<i>D</i>	25240	18458	43314	1286	22575	18666
<i>A</i>	14471	27632	2345	41895	22724	18586
<i>R</i>	14698	28463	20857	23851	1651	42149
<i>L</i>	21296	19245	18476	20873	41682	1399

the measurement of R_{pairs} , and P_{PPLN} is the down-conversion probability of the PPLN crystal. Here, P_{PPLN} includes the coupling loss from the pigtailed optical fiber into the PPLN crystal as well as any losses caused by the narrow wavelength acceptance of the PPLN waveguide (η_{in} and η_{CW} in Ref. [18], respectively).

During the measurements described in Sec. III, we obtain triplet coincidence rates of 8.3 ± 0.5 per hour. From these values, the effective down-conversion efficiency of the second crystal during the experiment is found to be $P_{\text{PPLN}} = (1 \pm 0.1) \times 10^{-6}$.

With a three-qubit tomography requiring measurements from 27 different bases, obtaining the counts for a reconstruction of the density matrix is not feasible in a reasonable amount of time, especially if we want to quantify the stability of the source. Instead we employ a GHZ witness [27] which

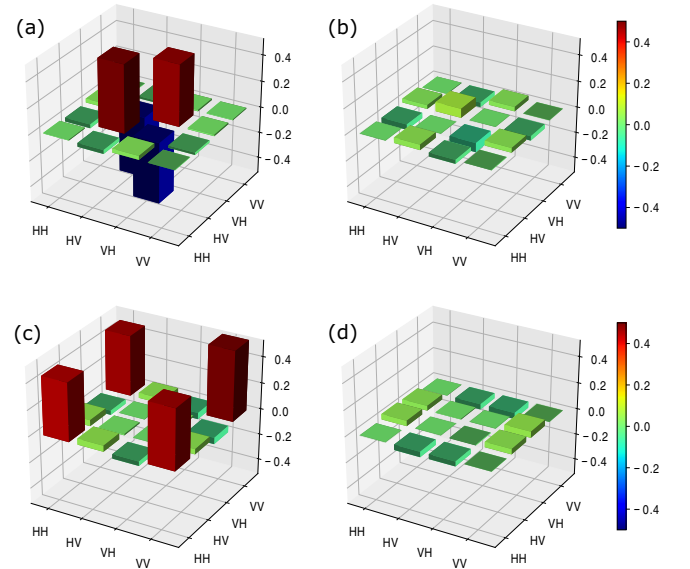


FIG. 3. Density matrix describing the state of polarization of both sources of entangled photon pairs. For the PPKTP source, the (a) real part and the (b) imaginary part of the density matrix. With a coincidence window of 0.5 ns, the resulting state has a $|\Psi^-\rangle$ fidelity of $96.45 \pm 0.01\%$, a purity of $95.61 \pm 0.03\%$ and a tangle [26] of $91.47 \pm 0.05\%$. For the PPLN source, we have the (c) real and (d) imaginary part of the density matrix, which was measured with a coincidence window of 0.3 ns. The resulting state has a $|\Phi^+\rangle$ fidelity of $95.06 \pm 0.05\%$, a purity of $93.7 \pm 0.1\%$, and a tangle of $86.6 \pm 0.2\%$.

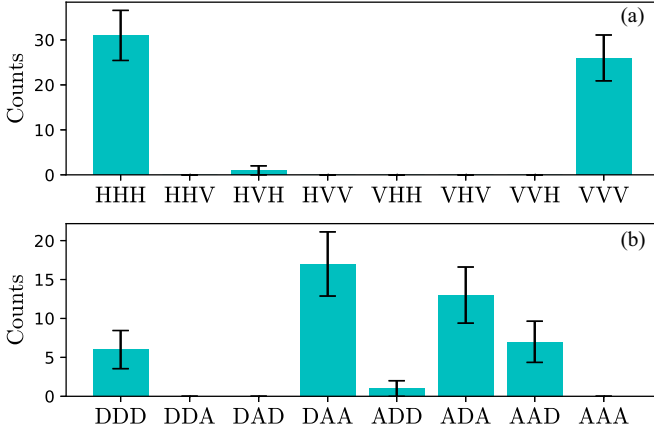


FIG. 4. Measured triple coincidence counts for the witness calculated in Table III. There are (a) 58 threefold coincidences in the σ_z basis and (b) 44 in the σ_x basis for a total of 102 coincidences in 16 h. Error bars are one standard deviation and calculated by assuming Poissonian count rates.

requires a measurement in just two bases and gives a lower bound on the fidelity of our state [28]. The witness is used for the GHZ state given in Eq. (1), and is given by

$$W_{\text{GHZ}} = \frac{3}{2} \cdot \mathbb{1}^3 - \sigma_x \otimes \sigma_x \otimes \sigma_x - \frac{1}{2} (\mathbb{1} \otimes \sigma_z \otimes \sigma_z + \sigma_z \otimes \mathbb{1} \otimes \sigma_z + \sigma_z \otimes \sigma_z \otimes \mathbb{1}), \quad (6)$$

where the σ represent their respective Pauli matrices. The lower bound of the fidelity between our experimental state and the GHZ state is given by

$$F_{\text{GHZ}} \geq \frac{1 - W_{\text{GHZ}}}{2}. \quad (7)$$

This witness is convenient as it only requires measurements in two measurement bases to obtain a lower bound on the fidelity of our state.

The measurements for the witness were taken over 16 h, with 8 h for each basis. Fifty-eight threefold coincidences were measured in the σ_z basis and 44 in the σ_x basis for a total of 102 coincidences in 16 h. This gives an average of 6.4 ± 0.6 triplets per hour. The measured triplet coincidence counts of this measurement are shown in Fig. 4 while the results of the witness are shown in Table III. The

TABLE III. Calculated witness results. The calculated errors are one standard deviation, calculated by assuming Poissonian noise on the triplet count rate.

Measurement	Value	Error
$\sigma_x \otimes \sigma_x \otimes \sigma_x$	0.95	0.05
$\mathbb{1} \otimes \sigma_z \otimes \sigma_z$	0.97	0.03
$\sigma_z \otimes \mathbb{1} \otimes \sigma_z$	1.00	0.04
$\sigma_z \otimes \sigma_z \otimes \mathbb{1}$	0.97	0.03
W_{GHZ}	-0.92	0.10
Lower bound of F_{GHZ}	0.96	0.05

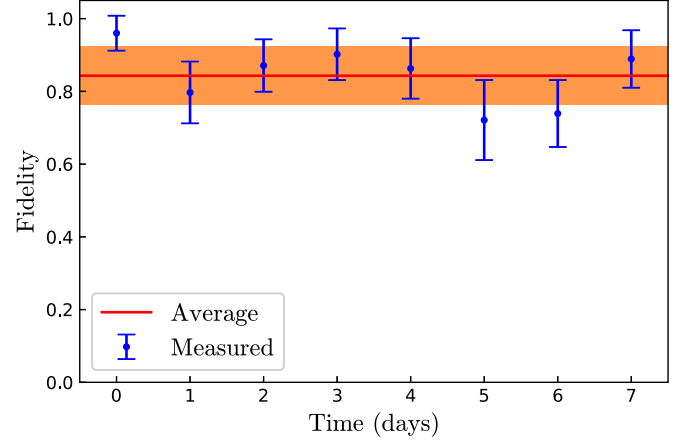


FIG. 5. Calculated lower bounds of fidelity over time. No adjustments were made to the source once the measurements began. Each of the two Pauli measurements lasted 8 h, followed by an 8-h downtime. The lower bound of the state fidelity begins at a maximum of $96 \pm 5\%$. Over the entire 7-day period, the average fidelity is $84 \pm 8\%$.

entanglement witness is violated convincingly with a value of $W_{\text{GHZ}} = -0.92 \pm 0.10$, confirming the entanglement of the state. This gives a minimum fidelity with the targeted GHZ state of $F_{\text{GHZ}} = 0.96 \pm 0.05$.

Based on preliminary measurements, the phase of this source tends to drift over time. We believe this is most likely due to the instability of optical elements found outside of the interferometers, as reoptimizing the phase through the QWP ϕ brings the fidelity back to a maximum value. In order to characterize the stability of the source without these corrections, the entanglement witness was measured repeatedly over a period of several days. During this time, no adjustments were made to the source. As shown in Fig. 5, while the fidelity of the state does display variations, we find that the fidelity stays above 72% during the entire week-long measurement, with an average fidelity of $84 \pm 8\%$, indicating that the source has the potential for passive long-term stability.

V. DISCUSSION

In terms of source quality, the short-term fidelity of 96% is excellent. Further improvement efforts should therefore be primarily focused on improving stability and production rates.

While further investigation is required to precisely isolate the source of instability, it is likely that the fibers at each end of the PPLN waveguide are partially responsible, due to the wavelength mismatch with the 77-nm photons. It is therefore likely that the wavelength instability could be improved through better thermal stabilization of this portion of the setup, or perhaps by pigtailed the PPLN waveguide with endlessly single-mode photonic crystal fibers [29], which would allow for single-mode operation at both 777 and 1550 nm.

As for the production rates, while the rates for C-SPDC are expected to be low, the experiment had additional limiting factors affecting the rates which are not inherent to the scheme. Indeed, previous experiments demonstrated entangled production rates of up to two orders of magnitude

higher than this work [21]. The difference is partially due to an additional coupling factor from I to P1 and P2 in Fig. 1, which lowers the expected triplet count rates by a factor of three. This loss could eventually be avoided by replacing the fiber from O to I with free space. A lower pump power in the first source, required to prevent damage to the superachromatic half-wave plates, accounts for a further factor of two. A novel approach to the Sagnac interferometer [30], removing the need for achromatic optics, could allow for higher pump intensities. The remaining difference in count rates is due to different coupling efficiencies to detectors 5–8. Importantly, none of these additional losses are fundamental to the current scheme, and could therefore be addressed with appropriate improvements to the setup. Alternatively, count rates could also be improved through the use of nonlinear crystals with higher conversion efficiencies [31].

With these further improvements to triplet production rates and stability, we expect this source to be of significant usefulness for applications requiring high-fidelity entangled photon triplets. In contrast to previous experiments creating three-photon polarization entanglement, our implementation does not rely on postselection, nor does it require active stabilization, thereby greatly reducing the complexity of the setup and making it attractive for applications requiring robust high-quality entanglement.

ACKNOWLEDGMENTS

We are grateful for the financial support from the Natural Sciences and Engineering Research Council of Canada, the Canadian Foundation for Innovation, Canada Research Chairs, and the New Brunswick Innovation Foundation.

-
- [1] J.-W. Pan, Z.-B. Chen, C.-Y. Lu, H. Weinfurter, A. Zeilinger, and M. Żukowski, Multiphoton entanglement and interferometry, *Rev. Mod. Phys.* **84**, 777 (2012).
- [2] M. Hillery, V. Bužek, and A. Berthiaume, Quantum secret sharing, *Phys. Rev. A* **59**, 1829 (1999).
- [3] M. Christandl and S. Wehner, Quantum anonymous transmissions, in *Lecture Notes in Computer Science* (Springer, Berlin, 2005), pp. 217–235.
- [4] D. E. Browne and T. Rudolph, Resource-Efficient Linear Optical Quantum Computation, *Phys. Rev. Lett.* **95**, 010501 (2005).
- [5] D. Bouwmeester, J.-W. Pan, M. Daniell, H. Weinfurter, and A. Zeilinger, Observation of Three-Photon Greenberger-Horne-Zeilinger Entanglement, *Phys. Rev. Lett.* **82**, 1345 (1999).
- [6] J.-W. Pan, M. Daniell, S. Gasparoni, G. Weihs, and A. Zeilinger, Experimental Demonstration of Four-Photon Entanglement and High-Fidelity Teleportation, *Phys. Rev. Lett.* **86**, 4435 (2001).
- [7] M. Eibl, S. Gaertner, M. Bourennane, C. Kurtsiefer, M. Żukowski, and H. Weinfurter, Experimental Observation of Four-Photon Entanglement From Parametric Down-Conversion, *Phys. Rev. Lett.* **90**, 200403 (2003).
- [8] M. Eibl, N. Kiesel, M. Bourennane, C. Kurtsiefer, and H. Weinfurter, Experimental Realization of a Three-Qubit Entangled W State, *Phys. Rev. Lett.* **92**, 077901 (2004).
- [9] Z. Zhao, Y. Chen, A. Zhang, T. Yang, H. Briegel, and J. Pan, Experimental demonstration of five-photon entanglement and open-destination teleportation, *Nature (London)* **430**, 54 (2004).
- [10] P. Walther, K. J. Resch, T. Rudolph, E. Schenck, H. Weinfurter, V. Vedral, M. Aspelmeyer, and A. Zeilinger, Experimental one-way quantum computing, *Nature (London)* **434**, 169 (2005).
- [11] C.-Y. Lu, X.-Q. Zhou, O. Gühne, W.-B. Gao, J. Zhang, Z.-S. Yuan, A. Goebel, T. Yang, and J.-W. Pan, Experimental entanglement of six photons in graph states, *Nat. Phys.* **3**, 91 (2007).
- [12] X.-C. Yao, T.-X. Wang, P. Xu, H. Lu, G.-S. Pan, X.-H. Bao, C.-Z. Peng, C.-Y. Lu, Y.-A. Chen, and J.-W. Pan, Observation of eight-photon entanglement, *Nat. Photonics* **6**, 225 (2012).
- [13] X.-L. Wang, L.-K. Chen, W. Li, H.-L. Huang, C. Liu, C. Chen, Y.-H. Luo, Z.-E. Su, D. Wu, Z.-D. Li, H. Lu, Y. Hu, X. Jiang, C.-Z. Peng, L. Li, N.-L. Liu, Y.-A. Chen, C.-Y. Lu, and J.-W. Pan, Experimental Ten-Photon Entanglement, *Phys. Rev. Lett.* **117**, 210502 (2016).
- [14] L.-K. Chen, Z.-D. Li, X.-C. Yao, M. Huang, W. Li, H. Lu, X. Yuan, Y.-B. Zhang, X. Jiang, C.-Z. Peng, L. Li, N.-L. Liu, X. Ma, C.-Y. Lu, Y.-A. Chen, and J.-W. Pan, Observation of ten-photon entanglement using thin BiB₃ O₆ crystals, *Optica* **4**, 77 (2017).
- [15] Y. Pilnyak, N. Aharon, D. Istrati, E. Megidish, A. Retzker, and H. S. Eisenberg, Simple source for large linear cluster photonic states, *Phys. Rev. A* **95**, 022304 (2017).
- [16] H.-S. Zhong, Y. Li, W. Li, L.-C. Peng, Z.-E. Su, Y. Hu, Y.-M. He, X. Ding, W. Zhang, H. Li, L. Zhang, Z. Wang, L. You, X.-L. Wang, X. Jiang, L. Li, Y.-A. Chen, N.-L. Liu, C.-Y. Lu, and J.-W. Pan, 12-Photon Entanglement and Scalable Scattershot Boson Sampling with Optimal Entangled-Photon Pairs From Parametric Down-Conversion, *Phys. Rev. Lett.* **121**, 250505 (2018).
- [17] D. M. Greenberger, M. A. Horne, A. Shimony, and A. Zeilinger, Bell's theorem without inequalities, *Am. J. Phys.* **58**, 1131 (1990).
- [18] H. Hübel, D. R. Hamel, A. Fedrizzi, S. Ramelow, K. J. Resch, and T. Jennewein, Direct generation of photon triplets using cascaded photon-pair sources, *Nature (London)* **466**, 601 (2010).
- [19] D.-S. Ding, W. Zhang, S. Shi, Z.-Y. Zhou, Y. Li, B.-S. Shi, and G.-C. Guo, Hybrid-cascaded generation of tripartite telecom photons using an atomic ensemble and a nonlinear waveguide, *Optica* **2**, 642 (2015).
- [20] S. Krapick, B. Brecht, H. Herrmann, V. Quiring, and C. Silberhorn, On-chip generation of photon-triplet states, *Opt. Express* **24**, 2836 (2016).
- [21] D. R. Hamel, L. K. Shalm, H. Hübel, A. J. Miller, F. Marsili, V. B. Verma, R. P. Mirin, S. W. Nam, K. J. Resch, and T. Jennewein, Direct generation of three-photon polarization entanglement, *Nat. Photonics* **8**, 801 (2014).
- [22] T. Kim, M. Fiorentino, and F. N. C. Wong, Phase-stable source of polarization-entangled photons using a polarization Sagnac interferometer, *Phys. Rev. A* **73**, 012316 (2006).
- [23] A. Fedrizzi, T. Herbst, A. Poppe, T. Jennewein, and A. Zeilinger, A wavelength-tunable fiber-coupled source of narrowband entangled photons, *Opt. Express* **15**, 15377 (2007).

- [24] H. C. Lim, A. Yoshizawa, H. Tsuchida, and K. Kikuchi, Stable source of high quality telecom-band polarization-entangled photon-pairs based on a single, pulse-pumped, short PPLN waveguide, *Opt. Express* **16**, 12460 (2008).
- [25] D. F. V. James, P. G. Kwiat, W. J. Munro, and A. G. White, Measurement of qubits, *Phys. Rev. A* **64**, 052312 (2001).
- [26] V. Coffman, J. Kundu, and W. K. Wootters, Distributed entanglement, *Phys. Rev. A* **61**, 052306 (2000).
- [27] G. Tóth and O. Gühne, Detecting Genuine Multipartite Entanglement with Two Local Measurements, *Phys. Rev. Lett.* **94**, 060501 (2005).
- [28] O. Gühne and G. Tóth, Entanglement detection, *Phys. Rep.* **474**, 1 (2009).
- [29] T. A. Birks, J. C. Knight, and P. S. Russell, Endlessly single-mode photonic crystal fiber, *Opt. Lett.* **22**, 961 (1997).
- [30] Y. S. Lee, M. Xie, R. Tannous, and T. Jennewein, Sagnac-type entangled photon source using only conventional polarization optics, *Quantum Sci. Technol.* **6**, 025004 (2021).
- [31] C. Wang, C. Langrock, A. Marandi, M. Jankowski, M. Zhang, B. Desiatov, M. M. Fejer, and M. Lončar, Ultrahigh-efficiency wavelength conversion in nanophotonic periodically poled lithium niobate waveguides, *Optica* **5**, 1438 (2018).